Virology 577 (2022) 149–154

Contents lists available at ScienceDirect

Virology

journal homepage: www.elsevier.com/locate/virology

Virion structure of Leishmania RNA virus 1

Michaela Procházková [a], Tibor Füzik [a], Danyil Grybchuk [a], Vyacheslav Yurchenko [b], Pavel Plevka [a,*]

[a] Central European Institute of Technology, Masaryk University, Kamenice 753/5, Brno, 625 00, Czech Republic
[b] Life Science Research Centre, Faculty of Science, University of Ostrava, Chittussiho 10, Ostrava, 710 00, Czech Republic

ARTICLE INFO

Keywords:
Virus
Viannia
Leishmaniasis
LRV1
Totiviridae
Structure
Cryo-electron microscopy
Capsid

ABSTRACT

The presence of Leishmania RNA virus 1 (LRV1) enables *Leishmania* protozoan parasites to cause more severe disease than the virus-free strains. The structure of LRV1 virus-like particles has been determined previously, however, the structure of the LRV1 virion has not been characterized. Here we used cryo-electron microscopy and single-particle reconstruction to determine the structures of the LRV1 virion and empty particle isolated from *Leishmania guyanensis* to resolutions of 4.0 Å and 3.6 Å, respectively. The capsid of LRV1 is built from sixty dimers of capsid proteins organized with icosahedral symmetry. RNA genomes of totiviruses are replicated inside the virions by RNA polymerases expressed as C-terminal extensions of a sub-population of capsid proteins. Most of the virions probably contain one or two copies of the RNA polymerase, however, the location of the polymerase domains in LRV1 capsid could not be identified, indicating that it varies among particles.

Importance.

Every year over 200 000 people contract leishmaniasis and more than five hundred people die of the disease. The mucocutaneous form of leishmaniasis produces lesions that can destroy the mucous membranes of the nose, mouth, and throat. *Leishmania* parasites carrying Leishmania RNA virus 1 (LRV1) are predisposed to cause aggravated symptoms in the mucocutaneous form of leishmaniasis. Here, we present the structure of the LRV1 virion determined using cryo-electron microscopy.

1. Introduction

Tropical areas around the globe are infested by parasites from the genus *Leishmania* (Kinetoplastea, Trypanosomatidae) (Akhoundi et al., 2016). *Leishmania* parasites are transmitted by the bite of an infected insect vector (Akhoundi et al., 2016). The disease can develop into four forms depending on the species of the parasite (Bruschi and Gradoni, 2018; Stuart et al., 2008): the cutaneous form with symptoms restricted to a self-healing ulceration, the mucocutaneous form that destroys the mucous tissues of the face, the visceral form (or kala-azar) which is lethal if untreated, and post-kala-azar dermal leishmaniasis, a complication of visceral leishmaniasis characterized by a discolored skin and rash. Together, the cutaneous and mucocutaneous forms cause 200 000 new cases annually.

The New World Leishmanias from the sub-genus *Viannia*, including *L. guyanensis* and *L. braziliensis*, often carry *Leishmania* RNA viruses (*Leishmaniavirus* spp., LRVs) (Guilbride et al., 1992; Widmer et al., 1989). The most common of them is LRV1 (Grybchuk et al., 2018a; Widmer et al., 1989). There is evidence that the presence of LRV1 promotes the metastatic behavior of the parasites and increases the likelihood of developing mucocutaneous leishmaniasis with aggravated symptoms (Adaui et al., 2016; Hartley et al., 2012; Ives et al., 2011; Kuhlmann et al., 2009). Furthermore, parasites carrying LRV1 are more likely to be resistant to treatments compared to the parasites without the virus (Adaui et al., 2016). In mice, LRV1-positive *L. guyanensis* caused larger footpad swelling and multiplied to higher numbers than the LRV1-negative strain (Ives et al., 2011). It was demonstrated that the presence of a viral symbiont disrupts the host interferon signaling, which leads to increased damage to the affected tissue (Rossi et al., 2017).

Only 10–15 virions of LRV1 are present in a cell (Kuhlmann et al., 2017; Robinson and Beverley, 2018) and there is no evidence for receptor-mediated cell entry for LRV1. Therefore, it was long thought that the virus is incapable of cell-to-cell transmission and instead is restricted to the cytoplasm of the infected cell (Armstrong et al., 1993). Nevertheless, recent observations of multiple simultaneous LRV1

* Corresponding author.
E-mail address: pavel.plevka@ceitec.muni.cz (P. Plevka).

https://doi.org/10.1016/j.virol.2022.09.014
Received 9 June 2022; Accepted 29 September 2022
Available online 1 November 2022

infections within a single *L. guyanensis* isolate (Tirera et al., 2017) as well as the discovery of the exosomal transfer of viruses between parasites (Atayde et al., 2019) suggest that virus spread is possible. However, these transfers are thought to be rare and only occur within local leishmania populations (Cantanhede et al., 2021).

The non-enveloped virion of LRV1 protects a linear 5283 nucleotide long double-stranded RNA genome in an icosahedral capsid (Scheffter et al., 1994). The icosahedral asymmetric unit contains two copies of a capsid protein that form distinct interactions with the rest of the capsid (Luque et al., 2018; Naitow et al., 2002). The particles include one or two copies of capsid proteins C-terminally extended by an RNA-dependent RNA polymerase domain (Grybchuk et al., 2018b; Kostygov et al., 2021; Lee et al., 1996). Transcription of the totivirus genome takes place inside the complete virions in the cytoplasm of infected cells (Castón et al., 1997; Luque et al., 2018). Newly synthesized positive-sense single-stranded RNA copies of the genome exit the particles to serve as mRNAs for translation and as genomic RNAs for the assembly of new virions (Castón et al., 1997; Luque et al., 2018). The LRV1 genome encodes two open reading frames, the coat protein and the RNA-dependent RNA polymerase (Stuart et al., 1992; Widmer et al., 1989). RNA-dependent RNA polymerases of totiviruses lack RNA capping activity (Ferron et al., 2012; Maga et al., 1995). It has been shown that transcripts of the L-A virus contain a 5' end diphosphate which may serve for the attachment of the cap by a cap-snatching mechanism (Fujimura and Esteban, 2011). The histidine 154 of L-A virus capsid protein covalently binds the yeast cap structure (m^7Gp) and adds it to the virus transcripts to prevent their degradation by the host cell (Blanc et al., 1994; Fujimura and Esteban, 2011, 2012). A similar process was described for the related L-BC ds RNA virus of yeast, suggesting that cap snatching is shared among fungal totiviruses (Fujimura and Esteban, 2013, 2019). However, the structure of an LRV1 virus-like particle demonstrated that the RNA-binding loop responsible for host RNA cap-binding and its transfer to viral RNA in the L-A virus is not conserved in LRV1 (Prochazkova et al., 2021).

There is an internal ribosomal entry site located at the 5' end of the virus mRNA that enables the initiation of translation of the totivirus capsid protein (Kim et al., 2005; Lee et al., 1996; Stuart et al., 1992). Translation of the LRV1 RNA-dependent RNA polymerase domain requires a +1 ribosomal frameshift, which occurs with a probability of 1–2% (Kim et al., 2005; Lee et al., 1996). As a result, LRV1 virions contain one or two copies of capsid proteins C-terminally extended by the RNA polymerase domain (Fujimura et al., 1992; Lee et al., 1996). However, the exact position of the polymerase domain in the LRV1 virion is not known. RNA polymerases of other viruses with dsRNA genomes replicated in their capsids that have been previously structurally characterized, including rotavirus, aquareovirus, Fako virus, bluetongue virus, *Pseudomonas* virus phi6, and cytoplasmic polyhedrosis virus, are positioned close to fivefold vertices of their capsids (Ding et al., 2019; Estrozi et al., 2013; He et al., 2019; Ilca et al., 2015; Jenni et al., 2019; Kaelber et al., 2020).

Here, we present the cryo-electron microscopy reconstructions of LRV1 virions and empty particles isolated from their natural host *Leishmania guyanensis*. The capsid of LRV1 is built from sixty dimers of capsid proteins organized with icosahedral symmetry. The location of the RNA-dependent RNA polymerase domains in the LRV1 capsid could not be identified, indicating that it may vary among particles.

2. Results and discussion

2.1. Structure of LRV1 virion and its comparison to that of virus-like particle

LRV1 virions and empty particles were isolated from *Leishmania guyanensis* promastigotes. The cryo-EM reconstructions of the LRV1 virion and empty particle were determined to resolutions of 4.0 and 3.6 Å, respectively (Fig. 1, S1, S2, Table 1). The maps of the capsids of the two particles are similar and can be superimposed with a correlation coefficient of 0.94. The capsid of LRV1 virion has an outer diameter of 431 Å, 7 Å larger than that previously reported for the virus-like particle (Prochazkova et al., 2021), because the virion structure contains an additional resolved surface loop. The thickness of the protein shell is 61 Å, and the diameter of the capsid cavity 309 Å. The capsid is assembled from 120 copies of capsid proteins organized with icosahedral symmetry, where the two subunits in the icosahedral asymmetric unit are in non-quasi-equivalent binding environments, an arrangement typical for totiviruses (Fig. 1C) (Dunn et al., 2013; Stuart et al., 1992). The two capsid protein subunits in the icosahedral asymmetric unit are, according to convention, named A and B. A subunits interact around the fivefold and twofold symmetry axes, whereas the B subunits form contacts at the threefold axes (Fig. 1C). The A and B subunits from one icosahedral asymmetric unit interact through an interface with a buried surface area of 1900 $Å^2$ (Fig. S3).

Table 1
Cryo-EM data and structure quality indicators.

Structure	LRV1 empty particle	LRV1 virion
EMDB	12558	14566
Magnification	105 000	75 000
Pixel size (Å)	1.340	1.063
Frames per exposure	40	39
Voltage	300 kV	300 kV
Electron dose ($e^-/Å^2$)	52	88
Symmetry	icosahedral	icosahedral
Initial particles (no.)	7912	7284
Particles used for reconstruction (no.)	3768	1156
Map resolution (Å)	3.63	4.02
FSC threshold	0.143	0.143
PDB ID	7NS2	7Z90
R factor	0.327	0.393
No. of non-hydrogen atoms in IASU[a]	9575	9575
RMSD bond lengths	0.007	0.007
Bad bonds (%)[b]	0	0
RMSD bond angles	0.864	0.809
Bad angles (%)[b]	0	0.1
Ramachandran favored (%)[b]	90.92	91.41
Ramachandran allowed (%)[b]	9.08	8.59
Ramachandran outliers (%)[b]	0	0
Poor rotamers (%)[b]	0	0
Clashscore (percentile)[b]	22.7 (91)	23.56 (89)
MolProbity score (percentile)[b]	2.37 (99)	2.37 (99)
Cβ deviations (%)[b]	0	0

[a] Icosahedral asymmetric unit.
[b] Values according to Molprobity.

LRV1 virion contains three types of openings in its capsid. The pores formed around fivefold and threefold symmetry axes have diameters of 8.8 Å and 6.3 Å, respectively (Fig. 2). Furthermore, an additional pore with a diameter of 6.0 Å is formed between two B and one A subunit (Fig. 2D). The dimensions of the pores are 20–30% smaller than those previously reported for the LRV1 virus like particles (Prochazkova et al., 2021), however, the structures are overall very similar, and the differences are caused by minor changes in the positions of the sidechains of the residues forming the pores. The pores on fivefold axes were speculated to be the exit channels for the newly synthesized RNA (Ding et al., 2019). Furthermore, all the pores in the capsid enable the entry of nucleotides to serve as a substrate for the genome replication that takes place inside the particle.

The capsid protein of LRV1 (743 amino acids) can be divided into the α- and β-domain (Fig. 3). The α-domain is comprised of α helices 1–12 and 16. The α helix 3 of A subunit mediates inter-subunit contacts around fivefold symmetry axes (Fig. 3). In contrast, in the B subunit the corresponding helix mediates an asymmetric interaction with the A subunit from the same icosahedral asymmetric unit. In both A and B subunits, α helix 10 forms the bottom of a positively charged groove which was speculated to play a role in the virus RNA capping process (Prochazkova et al., 2021). The β-domain is built from β strands that

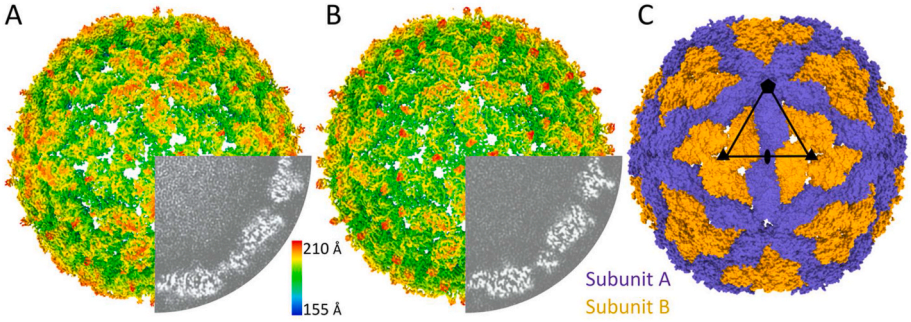

Fig. 1. Structures of LRV1 virion and empty particle. (AB) Surface representations of cryo-EM density maps of virion (A) and empty particle (B) rainbow colored according to the distance of the surface from the particle center. The bottom right quadrants of the maps are replaced with grayscale images of cryo-EM density distributions in the central sections of the particles. White indicates high values of density. **(C)** LRV1 virion with A subunits shown in purple and B subunits in orange. The positions of the selected icosahedral symmetry axes are indicated with a pentagon for fivefold, triangle for threefold, and oval for twofold. The black triangle shows the outline of an icosahedral asymmetric unit.

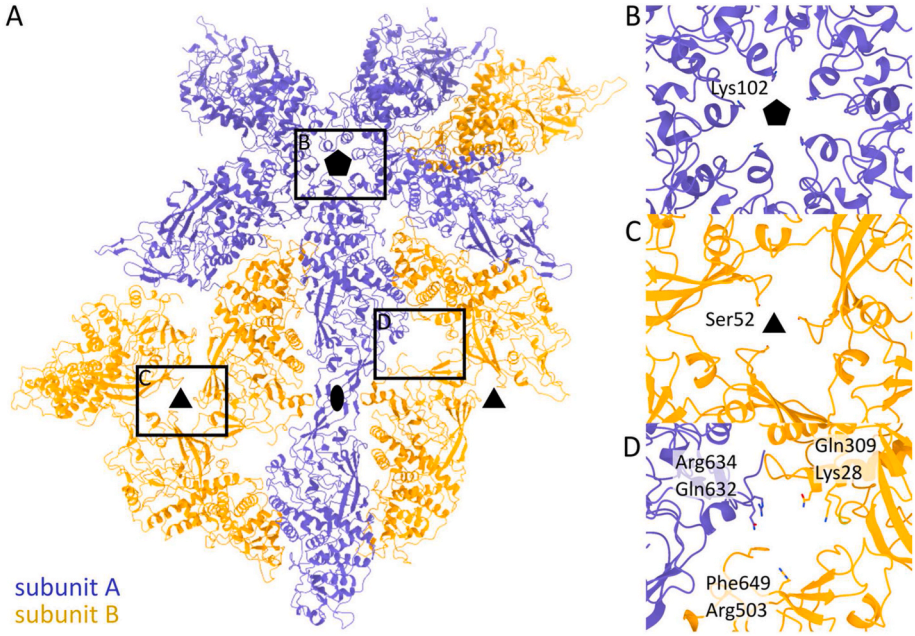

Fig. 2. Pores in LRV1 capsid. (A) Cartoon representation of a segment of LRV1 capsid. The capsid contains three major pores positioned on fivefold symmetry axes (B), threefold symmetry axes (C), and at the border of one A and two B subunits (D). Black rectangles indicate positions of the details shown in panels B–D. Positions of the selected icosahedral symmetry axes are indicated with a pentagon for fivefold, triangle for threefold, and oval for twofold. **(B–D)** Details of pores in LRV1 capsid. Sidechains of residues that determine the least pore diameters are shown in stick representation. (B) Pore on fivefold symmetry axis. (C) Pore on threefold symmetry axis. (D) Pore at the border of one A and two B subunits.

form four β sheets. The β sheet BALF from subunit A contacts the B subunit from the same asymmetric unit, however the β sheet BALF of subunit B interacts with another B subunit related by a threefold symmetry axis (Fig. 3). The AB loops of B subunits form the borders of the pores on threefold symmetry axes (Fig. 3). In both A and B subunits, the sheet DE faces the interior of the capsid. The sheets GHI and JK of A subunits interact with their counterparts in the A subunit related by a twofold symmetry axis. In contrast, the corresponding parts of the structure of B subunits contribute to contacts around threefold symmetry axes. The β-domains of both A and B subunits contain α helix 15 that faces the interior of the particle and helix 14 positioned between β sheets BALF and GHI at the center of the β-domain (Fig. 3).

The structures of icosahedral asymmetric units of LRV1 virion and that of the previously reported virus-like particle (PDB 6y83) (Prochazkova et al., 2021) can be superimposed with an RMSD of 0.66 Å for 596 C-α atom pairs available for the comparison. The structures differ in their peripheral loops. The structure of the LRV1 virion contains structured density for residues 205–209 between helices α 7 and 8 (Fig. 3) and C-terminal residues 636 and 637, which were not resolved in the virus-like particle. Subunit B of the LRV1 virion contains additional resolved residues 291–299 and 577–582 from the peripheral loops CD and JK, respectively, and C-terminal residues 643–649 (Fig. 3). The structure of residues 520–540 that form a surface loop in both A and B subunits could not be determined in either the virion or virus-like particle because of the limited resolution of the corresponding parts of the cryo-EM maps (Fig. S2). Flexible regions in structured proteins frequently serve as protein-protein recognition motifs (Coskuner-Weber and Uversky, 2019; Xue et al., 2012). We speculate that the 520–540 loop may enable the interaction of LRV1 with as-yet unknown cellular components or serve in rare events of LRV1 horizontal transfer.

2.2. Position of RNA polymerase in LRV1 virion

Virions of totiviruses contain one or two RNA-dependent RNA polymerases, and it has been shown that the replication of the LRV1 genome occurs inside virions (Castón et al., 1997; Fujimura et al., 1992). The RNA polymerase is expressed as a C-terminal extension of LRV1 capsid protein due to a +1 ribosomal frameshift (Kim et al., 2005). However, the position RNA polymerases in the capsid was not identified. Our attempts to determine the position of RNA polymerase in LRV1 virions and empty particles using asymmetric reconstructions of whole particles and asymmetric sub-particle reconstructions of decamers of capsid proteins were unsuccessful. The structure and function of RNA polymerase domains in cytoplasmic polyhedrosis virus from the family *Reoviridae* were studied using particles supplemented with nucleotides and S-adenosyl methionine (Cui et al., 2019). To detect the polymerase position in LRV1, we incubated the virions with ribonucleotides, however, we were unable to localize the RNA-dependent RNA polymerase inside the transcribing LRV1 virions. AlphaFold2 (Jumper et al., 2021) prediction of the structure of the LRV1 capsid protein extended by the polymerase domain shows that the two structured parts are linked by an 85-residue-long flexible linker. Therefore, it is likely that the extended

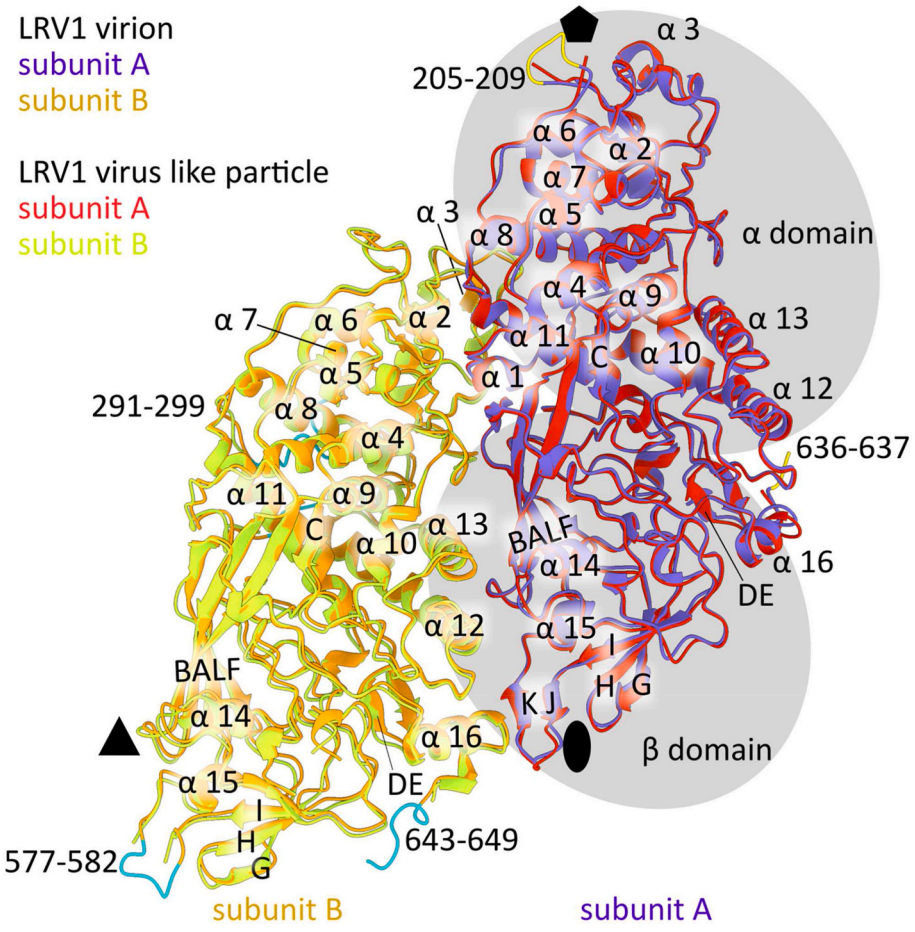

Fig. 3. Comparison of structures of icosahedral asymmetric units of LRV1 virion and virus-like particle. Capsid proteins are shown in cartoon representation. Subunits of the LRV1 virion are shown in purple (A subunit) and orange (B subunit) and those of the virus-like particle are shown in red (A subunit) and green (B subunit). Residues that are resolved in the virion structure, but not in that of the virus-like particle, are shown in yellow for the A subunit and cyan for the B subunit. Positions of the selected icosahedral symmetry axes are indicated with a pentagon for fivefold, triangle for threefold, and oval for twofold. The division of the A subunit into α and β-domains is indicated with background grey ovals.

capsid protein including the polymerase domain can be incorporated into capsids as either the A or B subunit, and the positions of the polymerase domain in the capsid vary from particle to particle.

3. Materials and methods

3.1. Leishmania growth and purification of LRV1

Leishmania guyanensis (MHOM/BR/75/M4147) promastigotes infected with LRV1 (Zangger et al., 2013) were grown at room temperature (22 °C) with mild orbital shaking in 1 l Flat-Sided Cell Culture Flasks (TPP) in M199 media buffered with 25 mM HEPES (pH 7.4) and supplemented with 10% fetal bovine serum, hemin (2 μg/ml), biotin (2 μg/ml) and penicillin-streptomycin antibiotic mix (all from Sigma-Aldrich) as described earlier (Podešvová et al., 2020). The identity of species was confirmed by diagnostic PCR as described previously (Yurchenko et al., 2006). Cells were grown to the early stationary phase (5×10^7 cells per ml), pelleted by centrifugation, flash-frozen in liquid nitrogen, and stored at −80 °C. The duration of continuous passaging was limited to one month, and the presence of the virus in the last passage was verified using RT-PCR as described previously (Brettmann et al., 2016).

A pellet of 3×10^{11} cells was resuspended in 50 ml of lysis buffer (50 mM HEPES pH 7.4, 150 mM NaCl, 2% Triton X-100, 1 mM $MgCl_2$, 1 mM $CaCl_2$, 10 μg/ml DNAse I, Roche protease inhibitor cocktail), incubated for 1 h at 4 °C, sonicated for 3 min using 2s pulse/10s pause at 80% amplitude with a Q700 sonicator (Qsonica) and cleared by centrifugation at 10 000 g, 4 °C for 10 min. The cleared lysate was mixed with 27 g of $CsCl_2$ and separated by ultracentrifugation at 275 000 g at 4 °C for 18 h in an SW 41 swing rotor (Beckman Coulter). Opaque bands containing the virus particles were extracted using a needle, and buffer-exchanged through 100 kDa cellulose Amicon filter device to HEPES buffer (50 mM HEPES pH 7.4, 150 mM NaCl). Samples of total lysate, cell debris, and soluble concentrated virus were analyzed by Western blot to verify the presence of LRV1 (Fig. S4). The virus was detected by a polyclonal antibody generated against in-house prepared recombinant LRV1 capsid protein (Davids Biotechnologie).

3.2. Cryo-electron microscopy and single-particle reconstruction

Four microliters of purified LRV1 virus solution were applied onto holey carbon grids (Cu, 300 mesh, R2/1; Quantifoil Micro Tools), blotted, and plunge frozen in liquid ethane using a Vitrobot Mark IV (Thermo Fisher Scientific) with the following settings: blot time 1 s, wait time 20 s, and blot force −2. Data were collected using a Titan Krios (Thermo Scientific) electron microscope operated at 300 kV and aligned for parallel illumination in nanoprobe mode. Individual images were recorded using a K2 Summit direct electron detector in super-resolution mode (50 $e^-/Å^2$) with underfocus values ranging from −0.5 to −3 μm at a nominal magnification of 105 000 x, resulting in a pixel size of 1.34 Å/px. Each image was recorded in movie mode and saved as 40 separate movie frames (dose 1.3 $e^-/Å^2$/frame). The frames from each exposure were aligned to compensate for drift and beam-induced motion during image acquisition using the program MotionCor2 (Zheng et al., 2017). 310 particles were manually selected using e2boxer.py from the software package EMAN2 (Tang et al., 2007) and used as a training set for crYOLO automated picking. crYOLO-picked particles were filtered at precision value 5 (Wagner et al., 2019; Wagner and Raunser, 2020). Contrast transfer function parameters for each micrograph were automatically estimated using the program CTFFIND4 (Rohou and

Grigorieff, 2015). The structure of the empty LRV1 particle was reconstructed using the package RELION 3.0 (Scheres, 2012). The initial model was generated from the structure of the LRV1 virus-like particle (PDB ID: 6y83), which was low-pass-filtered to 40 Å. The dataset was subjected to multiple-rounds of 2D and 3D classifications, Bayesian polishing, and Ewald sphere correction. The final reconstruction for the empty particle was performed using the program 3dautorefine. The resulting unfiltered electron density map was masked with threshold mask, which was prepared using the RELION mask_create function. The occurrence of overmasking was monitored by inspecting the shape of the FSC curve. Furthermore, the shapes of the FSC curves of phase-randomized half-datasets were checked, following the 'gold standard' procedure (Rosenthal and Henderson, 2003). The resolution of the final reconstruction was estimated as the value at which the FSC curves fell to 0.143 (Scheres and Chen, 2012). In parallel, purified LRV1 was mixed with the ribonucleotide mix (150 mM NaCl, 9 mM $MgCl_2$, 4 mM ATP, 2 mM GTP/CTP/UTP, 640 μM S-adenosylmethionine) (Cui et al., 2019) and incubated for 5 min at 37 °C. Four microliters of the sample were applied to an electron microscopy grid, blotted, and plunge frozen in liquid ethane using a Vitrobot Mark IV (Thermo Fisher Scientific) with the same settings as the previous sample. Data were collected using a Titan Krios (Thermo Scientific) electron microscope operated at 300 kV with a Falcon 3 direct detector with underfocus values ranging from −1 to −2.5 μm at a magnification of 75 000 x, resulting in a pixel size of 1.063 Å/px. Each image was recorded as 39 separate movie frames (dose 1.98 $e^-/Å^2$/frame), movies were aligned with MotionCor2. Contrast transfer function parameters for each micrograph were automatically estimated using the program CTFFIND4 (Rohou and Grigorieff, 2015). Individual particles were picked by crYOLO automated picking and filtered at a precision value of 5. The structure of the LRV1 virion was reconstructed using the package RELION 3.0. 3D classification was employed to select genome-containing particles. The reconstruction procedure was the same as that for the empty particle, but also included the classification of images into optics groups based on beam tilt, Bayesian polishing, and Ewald sphere correction.

3.3. Structure building and refinement

The structures of the empty LRV1 particle and LRV1 virion were built based on the structure of capsid proteins from an LRV1-virus-like particle (PDB ID:6Y83). The structures were refined using the combination of reciprocal space and real space refinements available in the Phenix package 1.18 (Liebschner et al., 2019).

Funding

This research was carried out under the project CEITEC 2020 (LQ1601), with financial support from the MEYS of the Czech Republic under National Sustainability Program II. This work was supported by IT4I project (CZ.1.05/1.1.00/02.0070), funded by the European Regional Development Fund and the national budget of the Czech Republic via the RDI-OP, as well as the MEYS via Grant (LM2011033). The research leading to these results received funding from the OP VVV program (CZ.02.1.01/0.0/0.0/16_019/0000759) and Czech Science Foundation grant 20-22689S to V.Y. and the project National Institute of Virology and Bacteriology (Program EXCELES, ID Project No. LX22NPO5103) - Funded by the European Union - Next Generation EU and Czech Science Foundation grant GX19–25982X to P.P.

Data availability

Cryo-EM electron density maps have been deposited in Electron Microscopy Data Bank (https://www.ebi.ac.uk/pdbe/emdb/) under accession numbers EMD-12558 (empty particle) and EMDB-14566 (native virion). The structure of the LRV1 empty particle and LRV1 virion have been deposited in Protein Data Bank (www.pdb.org) under PDB ID 7NS2 and 7Z90, respectively.

Declaration of competing interest

The authors declare that they have no known competing financial interests or personal relationships that could have appeared to influence the work reported in this paper.

Acknowledgement

We gratefully acknowledge the CEITEC Core Facility Cryo-Electron Microscopy and Tomography supported by the CIISB project LM2015043, funded by the MEYS of the Czech Republic.

Appendix A. Supplementary figures

Supplementary data to this article can be found online at https://doi.org/10.1016/j.virol.2022.09.014.

References

Adaui, V., Lye, L.F., Akopyants, N.S., Zimic, M., Llanos-Cuentas, A., Garcia, L., Maes, I., De Doncker, S., Dobson, D.E., Arevalo, J., Dujardin, J.C., Beverley, S.M., 2016. Association of the endobiont double-stranded RNA virus LRV1 with treatment failure for human leishmaniasis caused by leishmania braziliensis in Peru and Bolivia. JID (J. Infect. Dis.) 213, 112–121.

Akhoundi, M., Kuhls, K., Cannet, A., Votypka, J., Marty, P., Delaunay, P., Sereno, D., 2016. A historical overview of the classification, evolution, and dispersion of leishmania parasites and sandflies. PLoS Neglected Trop. Dis. 10, e0004349.

Armstrong, T.C., Keenan, M.C., Widmer, G., Patterson, J.L., 1993. Successful transient introduction of Leishmania RNA virus into a virally infected and an uninfected strain of Leishmania. Proc. Natl. Acad. Sci. U. S. A. 90, 1736–1740.

Atayde, V.D., da Silva Lira Filho, A., Chaparro, V., Zimmermann, A., Martel, C., Jaramillo, M., Olivier, M., 2019. Exploitation of the Leishmania exosomal pathway by Leishmania RNA virus 1. Nat Microbiol 4, 714–723.

Blanc, A., Ribas, J.C., Wickner, R.B., Sonenberg, N., 1994. His-154 is involved in the linkage of the Saccharomyces cerevisiae L-A double-stranded RNA virus Gag protein to the cap structure of mRNAs and is essential for M1 satellite virus expression. Mol. Cell Biol. 14, 2664–2674.

Brettmann, E.A., Shaik, J.S., Zangger, H., Lye, L.F., Kuhlmann, F.M., Akopyants, N.S., Oschwald, D.M., Owens, K.L., Hickerson, S.M., Ronet, C., Fasel, N., Beverley, S.M., 2016. Tilting the balance between RNA interference and replication eradicates Leishmania RNA virus 1 and mitigates the inflammatory response. Proc. Natl. Acad. Sci. U. S. A. 113, 11998–12005.

Bruschi, F., Gradoni, L., 2018. The Leishmaniases: Old Neglected Tropical Diseases.

Cantanhede, L.M., Mata-Somarribas, C., Chourabi, K., Pereira da Silva, G., Dias das Chagas, B., de Oliveira, R.P.L., Cortes Boite, M., Cupolillo, E., 2021. The maze pathway of coevolution: a critical review over the leishmania and its endosymbiotic history. Genes 12.

Castón, J.R., Trus, B.L., Booy, F.P., Wickner, R.B., Wall, J.S., Steven, A.C., 1997. Structure of L-A virus: a specialized compartment for the transcription and replication of double-stranded RNA. JCB (J. Cell Biol.) 138, 975–985.

Coskuner-Weber, O., Uversky, V.N., 2019. Alanine scanning effects on the biochemical and biophysical properties of intrinsically disordered proteins: a case study of the histidine to alanine mutations in amyloid-beta42. J. Chem. Inf. Model. 59, 871–884.

Cui, Y., Zhang, Y., Zhou, K., Sun, J., Zhou, Z.H., 2019. Conservative transcription in three steps visualized in a double-stranded RNA virus. Nat. Struct. Mol. Biol. 26, 1023–1034.

Ding, K., Celma, C.C., Zhang, X., Chang, T., Shen, W., Atanasov, I., Roy, P., Zhou, Z.H., 2019. In situ structures of rotavirus polymerase in action and mechanism of mRNA transcription and release. Nat. Commun. 10, 2216.

Dunn, S.E., Li, H., Cardone, G., Nibert, M.L., Ghabrial, S.A., Baker, T.S., 2013. Three-dimensional structure of victorivirus HvV190S suggests coat proteins in most totiviruses share a conserved Core. PLoS Pathog. 9.

Estrozi, L.F., Settembre, E.C., Goret, G., McClain, B., Zhang, X., Chen, J.Z., Grigorieff, N., Harrison, S.C., 2013. Location of the dsRNA-dependent polymerase, VP1, in rotavirus particles. J. Mol. Biol. 425, 124–132.

Ferron, F., Decroly, E., Selisko, B., Canard, B., 2012. The viral RNA capping machinery as a target for antiviral drugs. Antivir. Res. 96, 21–31.

Fujimura, T., Esteban, R., 2011. Cap-snatching mechanism in yeast L-A double-stranded RNA virus. Proc. Natl. Acad. Sci. U. S. A. 108, 17667–17671.

Fujimura, T., Esteban, R., 2012. Cap snatching of yeast L-A double-stranded RNA virus can operate in trans and requires viral polymerase actively engaging in transcription. J. Biol. Chem. 287, 12797–12804.

Fujimura, T., Esteban, R., 2013. Cap snatching in yeast L-BC double-stranded RNA totivirus. J. Biol. Chem. 288, 23716–23724.

Fujimura, T., Esteban, R., 2019. The cap-snatching reaction of yeast L-A double-stranded RNA virus is reversible and the catalytic sites on both Gag and the Gag domain of Gag-Pol are active. Mol. Microbiol. 111, 395–404.
Fujimura, T., Ribas, J.C., Makhov, A.M., Wickner, R.B., 1992. Pol of gag-pol fusion protein required for encapsidation of viral RNA of yeast L-A virus. Nature 359, 746–749.
Grybchuk, D., Kostygov, A.Y., Macedo, D.H., d'Avila-Levy, C.M., Yurchenko, V., 2018a. RNA viruses in trypanosomatid parasites: a historical overview. Mem. Inst. Oswaldo Cruz 113, e170487.
Grybchuk, D., Kostygov, A.Y., Macedo, D.H., Votypka, J., Lukes, J., Yurchenko, V., 2018b. RNA viruses in blechomonas (Trypanosomatidae) and evolution of leishmaniavirus. mBio 9.
Guilbride, L., Myler, P.J., Stuart, K., 1992. Distribution and sequence divergence of Lrv1 viruses among different leishmania species. Mol. Biochem. Parasitol. 54, 101–104.
Hartley, M.-A., Ronet, C., Zangger, H., Beverley, S.M., Fasel, N., 2012. Leishmania RNA virus: when the host pays the toll. Front. Cell. Infect. Microbiol. 2, 99.
He, Y., Shivakoti, S., Ding, K., Cui, Y.X., Roy, P., Zhou, Z.H., 2019. In situ structures of RNA-dependent RNA polymerase inside bluetongue virus before and after uncoating. P Natl Acad Sci USA 116, 16535–16540.
Ilca, S.L., Kotecha, A., Sun, X., Poranen, M.M., Stuart, D.I., Huiskonen, J.T., 2015. Localized reconstruction of subunits from electron cryomicroscopy images of macromolecular complexes. Nat. Commun. 6, 8843.
Ives, A., Ronet, C., Prevel, F., Ruzzante, G., Fuertes-Marraco, S., Schutz, F., Zangger, H., Revaz-breton, M., Lye, L.-f.L.-F., Hickerson, S.M., Beverley, S.M., Acha-Orbea, H., Launois, P., Fasel, N., Masina, S., 2011. Leishmania RNA virus controls the severity of mucocutaneous leishmaniasis. Science 331, 775–778.
Jenni, S., Salgado, E.N., Herrmann, T., Li, Z., Grant, T., Grigorieff, N., Trapani, S., Estrozi, L.F., Harrison, S.C., 2019. In situ structure of rotavirus VP1 RNA-dependent RNA polymerase. J. Mol. Biol. 431, 3124–3138.
Jumper, J., Evans, R., Pritzel, A., Green, T., Figurnov, M., Ronneberger, O., Tunyasuvunakool, K., Bates, R., Zidek, A., Potapenko, A., Bridgland, A., Meyer, C., Kohl, S.A.A., Ballard, A.J., Cowie, A., Romera-Paredes, B., Nikolov, S., Jain, R., Adler, J., Back, T., Petersen, S., Reiman, D., Clancy, E., Zielinski, M., Steinegger, M., Pacholska, M., Berghammer, T., Bodenstein, S., Silver, D., Vinyals, O., Senior, A.W., Kavukcuoglu, K., Kohli, P., Hassabis, D., 2021. Highly accurate protein structure prediction with AlphaFold. Nature 596, 583.
Kaelber, J.T., Jiang, W., Weaver, S.C., Auguste, A.J., Chiu, W., 2020. Arrangement of the polymerase complexes inside a nine-segmented dsRNA virus. Structure 28, 604–612 e603.
Kim, S.N., Choi, J.H., Park, M.W., Jeong, S.J., Han, K.S., Kim, H.J., 2005. Identification of the +1 ribosomal frameshifting site of LRV1-4 by mutational analysis. Arch Pharm. Res. (Seoul) 28, 956–962.
Kostygov, A.Y., Grybchuk, D., Kleschenko, Y., Chistyakov, D.S., Lukashev, A.N., Gerasimov, E.S., Yurchenko, V., 2021. Analyses of leishmania-LRV Co-phylogenetic patterns and evolutionary variability of viral proteins. Viruses 13.
Kuhlmann, F.M., Robinson, J.I., Bluemling, G.R., Ronet, C., Fasel, N., Beverley, S.M., 2009. Supporting Information for Antiviral screening indentifies adenosine analogs targeting the endogenous dsRNA LRV1 pahogenicity factor. Time 2, 3–5.
Kuhlmann, F.M., Robinson, J.I., Bluemling, G.R., Ronet, C., Fasel, N., Beverley, S.M., 2017. Antiviral screening identifies adenosine analogs targeting the endogenous dsRNA Leishmania RNA virus 1 (LRV1) pathogenicity factor. Proc. Natl. Acad. Sci. U. S. A. 114, E811–E819.
Lee, S.E., Suh, J.M., Scheffter, S., Patterson, J.L., Chung, I.K., 1996. Identification of a ribosomal frameshift in Leishmania RNA virus 1-4. J. Biochem. 120, 22–25.
Liebschner, D., Afonine, P.V., Baker, M.L., Bunkoczi, G., Chen, V.B., Croll, T.I., Hintze, B., Hung, L.W., Jain, S., McCoy, A.J., Moriarty, N.W., Oeffner, R.D., Poon, B.K., Prisant, M.G., Read, R.J., Richardson, J.S., Richardson, D.C., Sammito, M.D., Sobolev, O.V., Stockwell, D.H., Terwilliger, T.C., Urzhumtsev, A.G., Videau, L.L., Williams, C.J., Adams, P.D., 2019. Macromolecular structure determination using X-rays, neutrons and electrons: recent developments in Phenix. Acta Crystallogr. D 75, 861–877.
Luque, D., Mata, C.P., Suzuki, N., Ghabrial, S.A., Caston, J.R., 2018. Capsid structure of dsRNA fungal viruses. Viruses 10.
Maga, J.A., Widmer, G., Lebowitz, J.H., 1995. Leishmania rna virus 1-mediated cap-independent translation. Mol. Cell Biol. 15, 4884–4889.
Naitow, H., Tang, J., Canady, M., Wickner, R.B., Johnson, J.E., 2002. L-A virus at 3.4 Å resolution reveals particle architecture and mRNA decapping mechanism. Nat. Struct. Biol. 9, 725–728.
Podešvová, L., Leštinová, T., Horáková, E., Lukeš, J., Volf, P., Yurchenko, V., 2020. Suicidal leishmania. Pathogens 9.
Prochazkova, M., Fuzik, T., Grybchuk, D., Falginella, F.L., Podesvova, L., Yurchenko, V., Vacha, R., Plevka, P., 2021. Capsid structure of leishmania RNA virus 1. J. Virol. 95.
Robinson, J.I., Beverley, S.M., 2018. Concentration of 2'C-methyladenosine triphosphate by Leishmania guyanensis enables specific inhibition of Leishmania RNA virus 1 via its RNA polymerase. J. Biol. Chem. 293, 6460–6469.
Rohou, A., Grigorieff, N., 2015. CTFFIND4: fast and accurate defocus estimation from electron micrographs. J. Struct. Biol. 192, 216–221.
Rosenthal, P.B., Henderson, R., 2003. Optimal determination of particle orientation, absolute hand, and contrast loss in single-particle electron cryomicroscopy. J. Mol. Biol. 333, 721–745.
Rossi, M., Castiglioni, P., Hartley, M.A., Eren, R.O., Prevel, F., Desponds, C., Utzschneider, D.T., Zehn, D., Cusi, M.G., Kuhlmann, F.M., Beverley, S.M., Ronet, C., Fasel, N., 2017. Type I interferons induced by endogenous or exogenous viral infections promote metastasis and relapse of leishmaniasis. Proc. Natl. Acad. Sci. U. S. A. 114, 4987–4992.
Scheffter, S., Widmer, G., Patterson, J.L., 1994. Complete sequence of leishmania rna virus-1-4 and identification of conserved sequences. Virology 199, 479–483.
Scheres, S.H., Chen, S., 2012. Prevention of overfitting in cryo-EM structure determination. Nat. Methods 9, 853–854.
Scheres, S.H.W., 2012. RELION: implementation of a Bayesian approach to cryo-EM structure determination. J. Struct. Biol. 180, 519–530.
Stuart, K., Brun, R., Croft, S., Fairlamb, A., Gurtler, R.E., McKerrow, J., Reed, S., Tarleton, R., 2008. Kinetoplastids: related protozoan pathogens, different diseases. J. Clin. Invest. 118, 1301–1310.
Stuart, K.D., Weeks, R., Guilbride, L., Myler, P.J., 1992. Molecular organization of Leishmania RNA virus 1. Proc. Natl. Acad. Sci. U. S. A. 89, 8596–8600.
Tang, G., Peng, L., Baldwin, P.R., Mann, D.S., Jiang, W., Rees, I., Ludtke, S.J., 2007. EMAN2: an extensible image processing suite for electron microscopy. J. Struct. Biol. 157, 38–46.
Tirera, S., Ginouves, M., Donato, D., Caballero, I.S., Bouchier, C., Lavergne, A., Bourreau, E., Mosnier, E., Vantilcke, V., Couppie, P., Prevot, G., Lacoste, V., 2017. Unraveling the genetic diversity and phylogeny of Leishmania RNA virus 1 strains of infected Leishmania isolates circulating in French Guiana. PLoS Neglected Trop. Dis. 11, e0005764.
Wagner, T., Merino, F., Stabrin, M., Moriya, T., Antoni, C., Apelbaum, A., Hagel, P., Sitsel, O., Raisch, T., Prumbaum, D., Quentin, D., Roderer, D., Tacke, S., Siebolds, B., Schubert, E., Shaikh, T.R., Lill, P., Gatsogiannis, C., Raunser, S., 2019. SPHIRE-crYOLO is a fast and accurate fully automated particle picker for cryo-EM. Commun Biol 2.
Wagner, T., Raunser, S., 2020. The evolution of SPHIRE-crYOLO particle picking and its application in automated cryo-EM processing workflows. Commun Biol 3.
Widmer, G., Comeau, A.M., Furlong, D.B., Wirth, D.F., Patterson, J.L., 1989. Characterization of a RNA virus from the parasite Leishmania. Proc. Natl. Acad. Sci. U. S. A. 86, 5979–5982.
Xue, B., Dunker, A.K., Uversky, V.N., 2012. Orderly order in protein intrinsic disorder distribution: disorder in 3500 proteomes from viruses and the three domains of life. J. Biomol. Struct. Dyn. 30, 137–149.
Yurchenko, V., Lukes, J., Xu, X., Maslov, D.A., 2006. An integrated morphological and molecular approach to a new species description in the Trypanosomatidae: the case of Leptomonas podlipaevi n. sp., a parasite of Boisea rubrolineata (Hemiptera: rhopalidae). J. Eukaryot. Microbiol. 53, 103–111.
Zangger, H., Ronet, C., Desponds, C., Kuhlmann, F.M., Robinson, J., Hartley, M.A., Prevel, F., Castiglioni, P., Pratlong, F., Bastien, P., Muller, N., Parmentier, L., Saravia, N.G., Beverley, S.M., Fasel, N., 2013. Detection of leishmania RNA virus in leishmania parasites. PLoS Neglected Trop. Dis. 7.
Zheng, S.Q., Palovcak, E., Armache, J.P., Verba, K.A., Cheng, Y.F., Agard, D.A., 2017. MotionCor2: anisotropic correction of beam-induced motion for improved cryo-electron microscopy. Nat. Methods 14, 331–332.